frontiers | Frontiers in Ecology and Evolution

TYPE Original Research
PUBLISHED 05 January 2024
DOI 10.3389/fevo.2023.1297047

OPEN ACCESS

EDITED BY
Lei Deng,
Northwest A&F University, China

REVIEWED BY
Eloy Becares,
University of León, Spain
Qiuwen Chen,
Nanjing Hydraulic Research Institute, China

*CORRESPONDENCE
Lianghong Long
long_llh@163.com

RECEIVED 19 September 2023
ACCEPTED 12 December 2023
PUBLISHED 05 January 2024

CITATION
Ji D, Han Y, Long L, Xin X, Xu H, Qiu S, Meng J, Zhao X, Huang Y and Liu D (2024) Hypoxia and its feedback response to algal blooms and CH_4 emissions in subtropical reservoirs.
Front. Ecol. Evol. 11:1297047.
doi: 10.3389/fevo.2023.1297047

Hypoxia and its feedback response to algal blooms and CH_4 emissions in subtropical reservoirs

Daobin Ji[1,2], Yanxing Han[2], Lianghong Long[1,2*], Xiaokang Xin[3], Hui Xu[4], Siqian Qiu[1], Jianghuai Meng[2], Xingxing Zhao[1], Yanan Huang[1] and Defu Liu[2,5]

[1]Engineering Research Center of Eco-Environment in Three Gorges Reservoir Region, Ministry of Education, China Three Gorges University, Yichang, Hubei, China, [2]Hubei Field Observation and Scientific Research Stations for Water Ecosystem in Three Gorges Reservoir, China Three Gorges University, Yichang, China, [3]Changjiang Water Resources Protection Institute, Changjiang Water Resources Commission of the Ministry of Water Resources, Wuhan, China, [4]Architectural Engineering Institute, Hubei Three Gorges Polytechnic, Yichang Hubei, China, [5]Hubei Key Laboratory of River-Lake Ecological Restoration and Algal Utilization, Hubei University of Technology, Wuhan, China

Anthropogenic nutrient input stimulates surface eutrophication and algal blooms and thus exacerbates oxygen depletion and hypoxia in aquatic ecosystems. However, existing studies have paid little attention on the understanding of the feedback relationships among oxygen consumption, algal succession and greenhouse gas effect after river damming, particularly in Three Gorges Reservoir. This field work investigated the thermal stratification, water quality and phytoplankton in four tributaries (Pengxi Bay (PXB), Daning Bay (DNB), Shennong Bay (SNB), and Xiangxi Bay (XXB)) of the Three Gorges Reservoir (TGR) in spring (April 25-28, 2022), and explored the drivers of hypoxia and its feedback response to algal blooms and methane (CH_4) emissions. The results showed that during the observation period, DO, thermal stratification, and algal blooms were more severe in PXB. The high Chemical Oxygen Demand (COD_{Mn}) (11.27 mg•L^{-1}) and Dissolved Organic Carbon (DOC) content (7.56 mg•L^{-1}) in PXB were the main causes of the progressive hypoxia. Furthermore, stronger density stratification in PXB inhibited the vertical supply of DO and accelerated bottom hypoxia. But the downslope density current replenished bottom DO in the upper reaches of the DNB, SNB, and XXB. The CH4 concentration was generally higher in hypoxia zone, especially in where cyanobacteria are the dominant species (eg., PX03 and PX04). Dam construction led to the succession of algal-dominant species, exerting a significant influence on the river carbon cycle. The expansion of cyanobacterial blooms and the consequence of metabolic substrates increase are gradually increasing oxygen deprivation, even hypoxia, and enhancing CH_4 production in rivers. These findings suggest that the succession of algal-dominant species caused by river damming has a pronounced positive feedback effect on reservoir hypoxia processes and greenhouse effect.

KEYWORDS

dissolved oxygen stratification, hypoxia, algal bloom, greenhouse gas, TGR

1 Introduction

DO plays a key role in the biogeochemical cycle of surface waters and is a sensitive indicator of physical and biogeochemical changes in reservoir aquatic ecosystems (Wetzel, 2001). When waters enter an anaerobic state, aquatic organisms die in large numbers and the release of sediment-reducing pollutants (e.g., ammonia nitrogen, orthophosphate, iron, manganese, and sulfide) increases (Picard et al., 2019; Ding et al., 2022), further deteriorating water quality. With the increase of pollution loads in watersheds and the intensification of water eutrophication, water hypoxia has become a severe global ecological and environmental problem in reservoirs (Sun et al., 2021; Jaiswal et al., 2023). Focusing on the dynamic changes in DO in reservoirs has important significance for maintaining a good reservoir ecological environment and ensuring the safety of the urban water supply.

For a long time, in-depth studies have been conducted on the DO supply and consumption process in reservoirs, the influencing factors, and their ecological and environmental impacts. Early research found (Correll, 1999; Schindler, 2006) that the increase in external phosphorus load was the main reason for reservoir hypoxia, with the study of Lake Erie in the United States being the most representative (Rucinski et al., 2016) and that the eutrophication level and polluted sediments in the waters were important internal driving factors affecting the formation of hypoxic zones. However, as attempts were made to control the external load inputs of several lakes, such as in Lake Erie, without successfully resolving hypoxia, researchers gradually determined that reservoir hypoxia is the result of a combination of factors such as an increase in pollution load, thermal stratification, and hydrodynamic processes (Bocaniov et al., 2020; Zhang et al., 2020). DO stratification and its vertical variations largely depend on the thermal stratification pattern of a reservoir (Zhang et al., 2015).Although organic matter decomposition (Qu et al., 2022) and sediment oxygen consumption (Song et al., 2016) within the thermocline and hypolimnion are the internal causes for local hypoxia or even anaerobic conditions in waters, thermal stratification hinders the atmospheric reoxygenation of surface waters and the replenishment of oxygen to bottom waters through photosynthetic oxygen production (Li et al., 2019), which was also an important external factor leading to the occurrence of the DO Metalimnetic Oxygen Minimum (MOM) in the thermocline and hypoxia in the hypolimnion (Mi et al., 2020; Wen et al., 2022). The intra-annual variation in thermal stratification also provides regular conditions for the intra-annual evolution of DO as well as the formation, development, and termination of hypoxic zones (Zhang, 2015). In addition, Scholars (Liu et al., 2019) found that changes in reservoir topography were an important factor in determining the hydrodynamic conditions of a reservoir and therefore a key auxiliary condition affecting the formation of hypoxic zones in waters. In recent years, it has been found (Yan et al., 2017) that the oxygen-consuming decomposition of declining and sinking algae during blooms is another crucial factor exacerbating the process of hypoxia in bottom waters, and a hypoxic environment intensifies the production of GHGs such as CH_4 in waters, which in turn provides abundant carbon sources for algal growth, further promoting the formation of an intense cycle of algal blooms. The formation, development, and evolution of reservoir hypoxia is a complex physical, chemical, and biological process and is closely related to many factors, such as water temperature stratification, nutritional status, sediment pollution, algal blooms, and reservoir morphology (Wen et al., 2022). Accordingly, when studying the issue of reservoir hypoxia, it is necessary to consider the comprehensive impact of various factors and analyze the hypoxic zones and their driving factors as a whole system.

The TGR, as China's largest strategic freshwater resource reservoir, has been the focus of many scholars studying water quality and algal blooms in its tributary bays after its impoundment (Liu et al., 2016; Yang et al., 2017; Yang et al., 2022). Previous monitoring results (Zhang et al., 2009) show that the DO concentration in the TGR is generally higher than 6 $mg{\cdot}L^{-1}$, and there have been no occurrences of hypoxic or anaerobic conditions in the waters. However, with the increasing pollution load and eutrophication of the waters, severe hypoxic and anaerobic conditions have recently emerged in bays such as Xiaojiang in the TGR (Ji et al., 2022). These conditions have persisted for a long time and have had a widespread impact, leading to adverse ecological environmental consequences. This result is consistent with the exacerbation of anaerobic conditions in the bottom waters of most reservoirs worldwide due to global warming in recent years (Jane et al., 2021). Furthermore, it is worth noting that hypoxic and anaerobic waters are accompanied by severe algal blooms and GHG emissions, exhibiting significant spatial variations among different tributaries and different river sections. Recent research on the Yulin River of the TGR (Liu, 2019) has also indicated close relationships among water hypoxia, algal blooms, and GHG emissions, suggesting the existence of a strong positive feedback mechanism. The algal blooms in tributaries caused by reservoir storage lead to a decrease in carbon deposition in rivers and promote the release of CH_4, which aggravates the greenhouse effect of rivers and increases the frequency of cyanobacterial outbreaks, forming intense positive feedbacks. When the planktonic algae in a reservoir are dominated by cyanobacteria, the carbon cycle process in the reservoir is significantly enhanced (Xue et al., 2021). Recently, field monitoring has found that the dominant species of algal blooms in the TGR have gradually evolved from channel-type blooms such as Bacillariophyta and Dinophyta blooms in the early stage of reservoir storage to lake-type blooms dominated by cyanobacteria and Chlorophyta (Liu et al., 2016; Yang et al., 2017). Additional research is needed to determine whether this succession process, with cyanobacteria as the dominant species in algal blooms, is an important factor in promoting hypoxia in tributary bays. The newly emerging hypoxic and anaerobic conditions in the TGR may pose new challenges to the water environment and aquatic ecology of tributary bays.

Many studies have been carried out previously on the problem of algal blooms in the tributary bays of the TGR. Recently, several studies (Huang et al., 2015; Liu et al., 2021) have been conducted on GHG emissions in the context of carbon peaking and carbon neutrality. However, the spatial distribution differences in DO in tributary bays during the same period, as well as the underlying

relationships among algal blooms, GHG emissions, and different tributary bays, remain unclear. In this study, the water environment and aquatic ecology of different typical tributary bays (PXB, DNB, SNB, XXB) of the TGR were monitored in spring, and the differences in DO, hydrodynamics, and water quality of the different tributary bays were compared to determine the causes of the formation of hypoxic and anaerobic conditions in PXB and to explore the mechanism of the strong positive feedback among reservoir hypoxia, algal blooms, and GHG emissions. After this study, we can further deepen our understanding of the high risks area of water quality and algal blooms in TGR, and help to pollution control and management in watershed scale.

2 Materials and methods

2.1 Study area

In this study, four typical tributaries on the northern bank of the TGR were selected as the study area (Figure 1A). The Pengxi River, Daning River, Shengnong River and Xiangxi River are four tributary in the up-stream region of the Three Gorges Dam. Since the impoundment of the Three Gorges Reservoir, the water level has risen to 175 meters, and the various tributaries upstream of the dam have transformed from natural river channels to artificial reservoirs. Influenced by the backflow of the Three Gorges, the flow velocity in the watercourses has slowed down. The backwater of TGR intruding the up-stream formed calm bay at a water level of 175 m. (Lv et al., 2022) The PXB originates in Zhonggu Village, Baiquan Township, Kaixian County, and flows into the Yangtze River in Shuangjiang Town, Yunyang County. The urbanization of Kaizhou District in the upper reaches of PXB is occurring rapidly. The pollution from urban domestic sewage and nonpoint source pollution after rainfall is severe, resulting in poor water quality in the inflows from the upper reaches (Liu et al., 2020). The DNB originates from the southern foothills of the Daba Mountains in northwestern Wuxi County, Chongqing Municipality, and joins the Yangtze River at the estuary of Wuxia, Wushan County. In the DNB watershed, there are few industrial pollution sources; agricultural pollution sources and urban domestic sewage are the main pollution sources; and the water quality of the inflow from the upper reaches is better than that of the mainstream in the main reservoir area (Shen et al., 2010). The SNB originates on the southern slope of Shennongjia in Hubei Province and flows into the Yangtze River in Badong County. The XXB has two sources: the eastern source is in Luomadian, Shennongjia Forest District, and the western source is in the southern part of the Shennongjia Mountains. The eastern and western rivers converge at Xiangtan in front of Zhaojun Village, Gaoyang Town, Xingshan County, and at this point, the rivers are referred to as the Xiangxi River, which

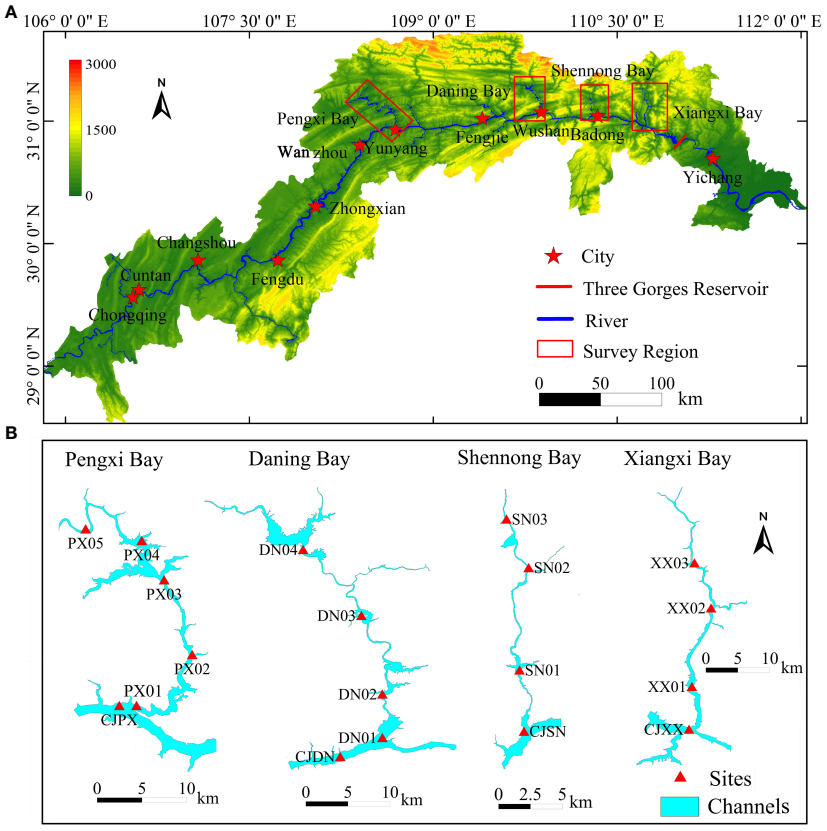

FIGURE 1
Layout of the monitoring sites of the typical tributary bays in the TGR area **(A)** is Water system map of Three Gorges reservoir in the study area, **(B)** is the layout of sampling points in each tributary bay.

flows into the Yangtze River at Xiangxi Village, Quyuan Town, Zigui County. The PXB, DNB, and SNB channels all generally exhibit alternating increases and decreases in width, showing transitional water environmental characteristics, while XXB has a straight and narrow channel, displaying channel-type environmental characteristics. The basic characteristics of the study area, such as drainage area, distance from estuary to dam, length of backwater area and backwater area, are shown in Table 1. All four tributaries are primary tributaries on the northern bank of the TGR. Due to their different distances from the TGR and different terrains, there are significant differences in their water environmental characteristics.

In this study, the monitoring of the water environment, sediments, and GHGs was carried out in tributary bays (PXB, DNB, SNB, and XXB) on the northern bank of the TGR from April 25 to 28, 2022. Four to five monitoring sites were set up in the surface, subsurface and bottom reaches of each tributary bay, and one monitoring site was set up in the mainstream of the Yangtze River at the estuary of each tributary. The specific layout of the monitoring sites is shown in Figure 1B.

2.2 Field monitoring and method

2.2.1 Field samplings

On-site monitoring was carried out using a multiparameter water quality analyzer (YSI-EXO,USA; error range<5%; Where the water temperature range is -5 to 50°C, the resolution ratio is 0.001° C; the DO range is 0 to 50 mg·L^{-1}, the resolution ratio is 0.01 mg·L^{-1}; the SpCond range is 0 to 200 mS/cm, the resolution ratio is 0.0001mS/cm; the Chl-a range is 0 to 400 μg/L, the resolution ratio is 0.01 μg/L; the range of depth is 0~250 m, the resolution ratio is 0.001m) from the United States to measure parameters such as water temperature (WT), DO, Specific Conductance (SpCond), Chlorophyll-a (Chl-a), and water depth (Depth) in the water environment. Photosynthetically active radiation (PAR) was determined using the underwater quantum sensor (LI-1400, USA) from the United States. In this study, the depth of water that differs from the surface temperature by less than 0.5°C was defined as the mixed layer depth (Z_{mix}), and the depth at which 1% of the PAR exits from the water surface was defined as the euphotic layer depth (Z_{eu}) (Siegel et al., 2002). Additionally, we utilized a handheld weather station to monitor on-site temperature, humidity, and wind speed(PH-HB-CJ2, China; the range of temperature is -50 to 80°C, and the resolution ratio is 0.1°C; the range of humidity is 0 to 100%, the resolution ratio is 0.1%; the range of wind speed is 0 to 45 m·s^{-1}, and the resolution ratio is 0.1 m·s^{-1}), and a Secchi disk was used to measure water transparency.

2.2.2 Laboratory experiment

One liter of surface water was collected for microscopic examination of phytoplankton. On-site, the water sample containing algae was fixed with an appropriate amount of Lugol's reagent and stored in the dark. After bringing the samples back to the laboratory, they were allowed to settle for 48 hours and then concentrated to 50 milliliters. Phytoplankton were classified and counted under an optical microscope. Using a stratified water sampler, one liter water samples were collected from the surface (0.5 meters below the water surface), subsurface, and bottom layers (0.5 meters above the sediment). The water samples were pretreated following national standards, and the determination of total nitrogen (TN), nitrate nitrogen(NO_3^--N), ammonium nitrogen (NH_4^+-N), total phosphorus (TP), COD_{Mn}, and DOC of the water was conducted in the laboratory. The specific determination methods are described in Table 2.

We collected 2 liters of sediment using a grab sampler, mixed the sample thoroughly, and placed it in a self-sealing bag. After removing the air, we brought the samples back to the laboratory for the determination of sediment total nitrogen (S-TN) and total organic carbon (S-TOC). The specific measurement methods are described in Table 2. We used a cylindrical sampler (SWB-1) to collect columnar sediment. At the field site, the samples were sealed with silicone plugs and transported back to the laboratory, where they were stored in a 4°C refrigerator for subsequent oxygen demand simulation experiments. The experimental procedures and methods are described in Section 2.3.1. The GHGs were collected using the headspace equilibration method. We used a 500 mL syringe, added 200 mL of high-purity nitrogen gas to the headspace, and then introduced 300 ml of bubble-free water sample. The syringe was vigorously shaken for 10 min under sealed conditions to achieve equilibrium between the CH_4 and carbon dioxide (CO_2) in the water and the headspace gas phase (equilibrium between the gas and liquid phases). The headspace gas was collected in vacuum-sealed aluminum foil bags that were prepared in advance, and the temperature of the water's headspace was noted after shaking. In the laboratory, the concentrations of methane and carbon dioxide gases were determined using greenhouse gas analyzer (Picarro G2201-i, the range of CH_4 is 0 to 655 mg·m^{-3}, and the resolution ratio is 0.7 mg·m^{-3}; the range of CO_2 is 180 to 7198 mg·m^{-3}, the resolution ratio is 1.8 mg·m^{-3}).

TABLE 1 The basic characteristics of the study area.

Tributaries	Drainage area (km^2)	Distance from estuary to dam(km)	Length of backwater area(km)	Backwater area (km^2)
PXB	3183	247.0	100.1	82.7
DNB	4050	122.5	59.3	32.4
SNB	1047	69.6	25.8	9.8
XXB	3099	34.5	38.8	18.4

TABLE 2 Methods for measuring physical and chemical factors.

Category	Indicators	Method	Standards
Water	TN	Alkaline potassium persulfate ultraviolet spectrophotometry	HJ636-2012
	NH_4^+-N	Nessler's reagent spectrometry	HJ535-2009
	NO_3^--N	Ultraviolet spectrophotometry	HJ/T346-2007
	TP	Ammonium molybdate spectrophotometry	HJ671-2013
	COD_{Mn}	Potassium permanganate titration	STAS 9887-1974
	DOC	Carbon and nitrogen element analyzer (multi N/C 3100, Germany)	/
Sediment	S-TN	Alkaline Potassium persulfate ultraviolet spectrophotometry	GB/T 32737-2016
	S-TOC	Carbon and nitrogen element analyzer (multi N/C 3100, Germany)	/

2.3 Data analysis methods

We processed and analyzed the raw data using Excel in Office (Microsoft, Redmond, USA). The research area and sampling point distribution map were created using ArcGIS 10.3 and Surfer 16. The spatial distribution of various indicators was plotted using MATLAB 2018a software (Mathworks, USA). The vertical distribution characteristics of environmental factors, mixing ratios, and physicochemical indicators were plotted using Origin 2018 software (OriginLab, Northampton, USA). The correlation analysis between DO and other physicochemical indicators was conducted using SPSS 26.0 software (IBM, Armonk, NY, USA). Significance is reported at the $p< 0.05$ and $p< 0.01$ levels. The calculation methods for the sediment oxygen consumption rate, water stability coefficient in this study are as Section 2.3.1 and 2.3.2.

2.3.1 Sediment oxygen demand

The sediment oxygen consumption rate was determined using the short-core incubation method (Cao et al., 2022). For the overlying water of the sediment, ultrapure water was used instead of *in situ* water. The cylindrical sediment samples were incubated in a temperature-controlled dark biochemical incubator at 20°C for 48 hours. DO concentration was continuously monitored using a dissolved oxygen sensor (HOBO Dissolved Oxygen Logger, HOBO, Canada, the range of DO is 0~30 $mg{\cdot}L^{-1}$, the resolution ratio is 0.02 $mg{\cdot}L^{-1}$). To address the issues of poor device sealing and long measurement cycles in traditional methods, a small chamber was attached to the end of the DO sensor, and the sensor probe was inserted into the chamber (referred to as the device). By measuring the variation in DO in the closed chamber over time, the sediment oxygen consumption rate was obtained. The specific procedure was as follows: (1) The overlying *in situ* water was slowly removed from the cylindrical sediment, and ultrapure water (DO: 6-8 $mg{\cdot}L^{-1}$) was slowly injected along the inner wall of the cylinder to avoid disturbing the surface sediment. (2) The device was slowly placed into the sediment sample, the DO sensor was vertically moved, the small chamber was positioned exactly on top of the sediment to form a sealed compartment, the device was fixed in place, and the sample was transferred to the incubator for temperature incubation. The sediment oxygen consumption (SOC) rate (Song et al., 2016) was calculated as Equation 1:

$$SOC = (k_c - k_w) \cdot \frac{V}{A} \cdot 24 \tag{1}$$

where SOC is the oxygen consumption rate of sediment ($mg{\cdot}m^{-2}{\cdot}d^{-1}$); $k_C = \frac{\Delta DO_C}{t}$; $k_w = \frac{\Delta DO_w}{t}$; ΔDO_C the difference in dissolved oxygen in the overlying water of sediment before and after cultivation ($mg{\cdot}L^{-1}$), ΔDO_w is the oxygen consumption difference of ultrapure water; t is the number of experimental cultivation hours (h); V is the device cavity volume (121.3 cm^3) and A is the cross-sectional area (16.6 cm^2).

2.3.2 Coefficient of water stability

Based on previous studies, this article disregarded the influence of sediment on water density and calculated the density of water (ρ) at different temperatures which was calculated as Equation 2 (Zhang et al., 2015):

$$\rho = 1000[1 - \frac{T + 288.9414}{508929.2(T + 68.12963)}(T - 3.9863)^2] \tag{2}$$

The stratification strength and stability during the thermal stratification period of the reservoir are characterized by the relative water column stability Index (RWCS) of the water body (Liu et al., 2019), and the calculation formula for RWCS is shown as Equation 3:

$$RWCS = \frac{\rho_b - \rho_s}{\rho_4 - \rho_5} \tag{3}$$

where ρ_b represents the density of the bottom layer water, ρ_s represents the density of the surface water, and ρ_4 and ρ_5 represent the densities of water at 4°C and 5°C respectively.

3 Results

3.1 Spatial difference in dissolved oxygen

The vertical distribution of DO in each tributary bay is shown in Figure 2. At the end of April, the spatial distributions of DO in the four tributary bays were significantly different. In PXB, the lower reaches exhibited no distinct stratification, while the middle and upper reaches displayed strong stratification. The waters in the middle to upper reaches of the bay demonstrated a certain degree of hypoxia. Near the estuary of PXB (PX01 ~ PX02), the vertical DO

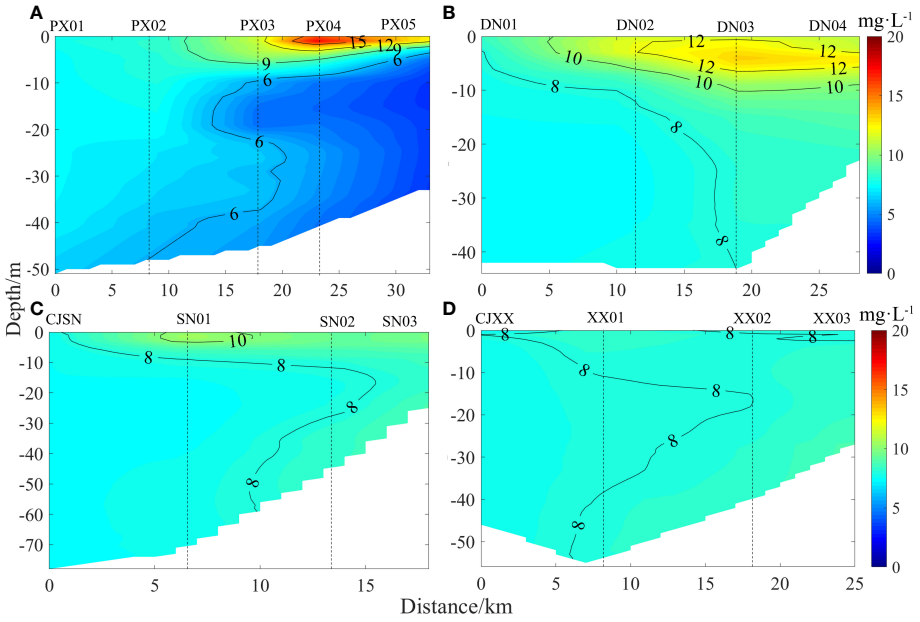

FIGURE 2
Spatial distribution of DO in the different tributary bays (**A**, PXB; **B**, DNB; **C**, SNB; **D**, XXB).

remained relatively constant at approximately 8.00 mg·L^{-1}. However, in the middle and upper reaches (PX03 ~ PX05), the DO near the surface was supersaturated (with a DO saturation concentration of 8.41 mg·L^{-1} at a water temperature of 24°C), decreased sharply between the depths of 5 to 9 m, and reached a minimum between 9 and 20 m (with a DO concentration of only 3.45 mg·L^{-1} at PX04). The DO slightly increased in the bottom waters, however, the subsurface and bottom waters of the bay remained in a hypoxic state. In contrast, DNB's surface waters were saturated with DO (> 10.00 mg·L^{-1}) throughout. The DO concentration peaked at a depth of 5 m (DN03, 13.30 mg·L^{-1}), decreased slightly with increasing depth, but remained higher than 8.00 mg·L^{-1} throughout the bay, indicating an overall oxygen-rich state (with a DO saturation concentration of 8.73 mg·L^{-1} at a water temperature of 22°C). SNB and XXB exhibited similar patterns, with little spatial difference in their DO concentrations. In SNB, the DO concentration near the surface (0-2 m) was approximately 10 mg·L^{-1}, peaking at SN01 (10.53 mg·L^{-1}), and maintained at about 8 mg·L^{-1} below 2 m with little vertical difference. In XXB, the vertical distribution of DO was evenly mixed and remained at approximately 8.0 mg·L^{-1}, showing no significant vertical variation.

3.2 Thermal stratification features

Figure 3 depicts the spatial distributions of water temperature in each of the four representative tributary bays of the TGR. Generally, from surface to bottom, the water temperature ranges were as follows: 16.48-25.89°C, 15.30-23.47°C, 15.22-21.86°C, and 13.29-22.06°C, respectively. The closer the measurements were taken to the upper reaches of a tributary bay, the higher the water temperature, leading to more pronounced water temperature stratification. In PXB and DNB, water temperature stratification was slight in the estuary and at the ends of the upper reaches but strong in the middle reaches. For instance, the RWCS indicators of PXB were ordered as: PX05(86.90)< PX02(87.90)< PX03(163.40)< PX04(235.30). The vertical water temperature in the middle reaches of these two tributaries presented a three-layer structure: "Mixed layer-Thermocline-Hypolimnion". (1) In PXB, the near-surface layer had high water temperature, with Z_{mix}<1 m in the near-surface layer of the middle and upper reaches of the river (Supplementary Figure S1). The water temperature dropped rapidly within a water depth of 2-5 m (with the maximum vertical temperature gradient reaching 3.58 °C·m^{-1}), and stabilized within a water depth of 5-50 m. (2) In DNB, the near-surface waters reached Z_{mix} at 2-3 m (Supplementary Table S1), and the water temperature decreased rapidly at a depth of 3-5 m (with a maximum temperature gradient of 2.60°C·m^{-1}) and stabilized within a depth of 5-44 m, with lower temperature in the bottom waters. (3) In the estuary of SNB, water temperature was completely mixed (Z_{mix} = 39 m) and was always between the surface and bottom temperature difference. The reservoir bay showed weak thermal stratification, with the maximum vertical temperature gradient being only 0.60°C·m^{-1}. (4) In XXB, thermal stratification was weak with no clear thermocline, and Z_{mix} reached 5 m in the near-surface layer, while the euphotic zone, Z_{eu}, reached 15 m (Supplementary Figure S1). In the upper reaches of DNB, SNB, and XXB, there were obvious low-temperature downslope flows at the bottom, with a water temperature of approximately 16°C. SpCond, indicative of the concentration of dissolved salts in water, is commonly used as a tracer for exchange processes in different water types. As shown in the spatial distribution of SpCond (Supplementary Figure S2), the main-stream of Yangtze generally exhibited a backward flow, submerging into the bays from the

10.3389/fevo.2023.1297047

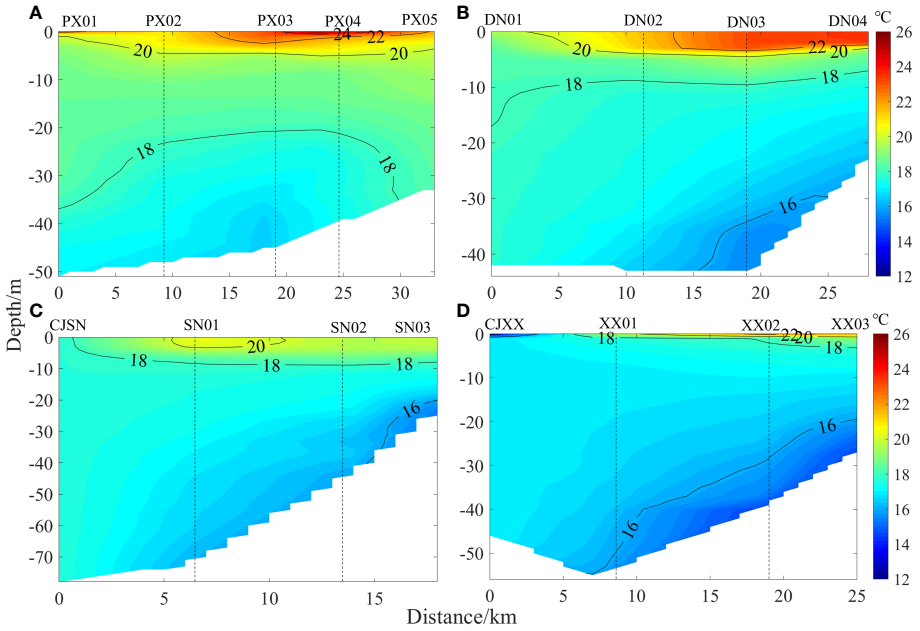

FIGURE 3
Spatial distribution of water temperature in the different tributary bays (**A**, PXB; **B**, DNB; **C**, SNB; **D**, XXB).

subsurface layer. The backflow gradually decreased from the estuary to the upper reaches. The inflow from the upper reaches of PXB exited the bay from the surface layer, whereas in DNB the inflow flowed from the surface and bottom layers to the main-stream of the Yangtze Bay in a stratified density flow. The inflow from the upper reaches of SNB and XXB submerged into the bottom in the form of downslope density flow.

3.3 Spatial distribution of phytoplankton

The concentrations of Chlorophyll a (Chl-a) in the surface layer of various tributary bays of the TGR during the observation period are depicted in Figure 4A. Notably, severe cyanobacteria (Figure 4B, PX03) and Dinophyta (Figure 4C, PX05) were observed in PXB, while DNB showed no significant bloom activity (considering a chlorophyll threshold of 30 μg·L^{-1} for bloom outbreaks). Chl-a observations highlighted an obvious spatial variation in the surface Chl-a concentrations within PXB. The surface Chl-a concentration remained extremely low, approximately 1.00 μg·L^{-1}, at monitoring sites ranging from CJPX to PX02. However, the Chl-a concentrations from PX03 to PX05 exceeded the threshold for algal blooms (30 μg·L^{-1}) (Zhang et al., 2011). It was noted that the closer the measurement site was to the upper reaches, the more severe the blooms were, with the Chl-a concentration in the surface layer at PX05 peaking at 231.77μg·L^{-1}. In contrast, DNB exhibited a pattern of high Chl-a concentration in the surface layer of the upper reaches, with surface Chl-a concentrations being quite low (0.52-

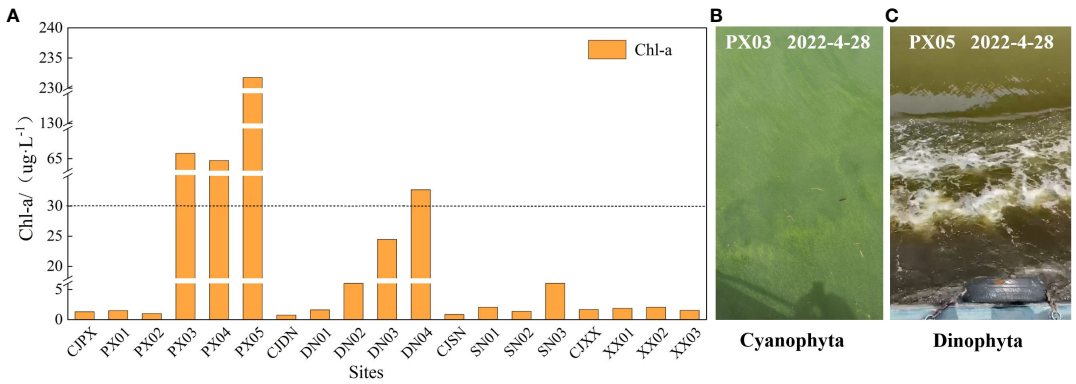

FIGURE 4
Surface chlorophyll a concentration at the different monitoring sites **(A)** is the distribution of Chl-a at each monitoring site, **(B)** is the cyanobacteria bloom of PX03, and **(C)** is the dinoflagellate bloom of PX05.

10.3389/fevo.2023.1297047

6.17 μg·L^{-1}) from CJDN to DN02. However, the highest concentration was recorded at DN04, reaching 35.26 μg·L^{-1}, thereby surpassing the threshold of algal bloom outbreaks.

To further analyze the characteristics of algal bloom outbreaks in tributary bays, we carried out microscopic examinations of phytoplankton on the surface of the four tributary bays. The algal density composition results shown in Figure 5 indicate that the maximum total algal density in PXB was as high as 420.21×10^4 L^{-1}, significantly higher than the maximum total algal density in DNB (80.00×10^4 L^{-1}). A total of 5 phyla and 15 genera of phytoplankton species were identified in the four tributary bays, namely Dinophyta (1 genus), Cryptophyta (1 genus), Cyanophyta hyta (4 genera), Chlorophyta (5 genera), and Bacillariophyta (4 genera). Cyanobacteria constituted the highest proportion (57.10%) of the total number of phytoplankton, followed by dinoflagellates (32.00%). The dominant algal species and spatial differences in the four tributary bays were evident. In PXB, cyanobacteria dominated (99.59%) the middle reaches (PX03). The phytoplankton biomass at PX04 and PX05 in the upper reaches was similar, approximately 134-140×10^4 L^{-1}, with the dominant algal species gradually transitioning from cyanobacteria to dinoflagellates. Specifically, dinoflagellates and cyanobacteria constituted approximately 64.71% and 33.13% at PX04, respectively, and about 85.36% and 13.69% at PX05. In DNB, dinoflagellates were the dominant species (81.25%), with Chlorophyta was the second most dominant species (14.06%) in the upper reaches (DN04). As one approached the estuary, Bacillariophyta gradually became the dominant species, accounting for 72.73% at the estuary (CJDN), although their biomass was not high. In SNB, the cyanobacterial biomass was comparable at the different monitoring sites. The closer the site was to the upper reaches, the higher the diatom biomass, however the total algal biomass was low. In XXB, which had the lowest biomass, cyanobacteria were dominant near the estuary (XX01), and cryptophytes dominated in the upper reaches (XX03).

3.4 Water quality and sediment properties

Figure 6 shows the distribution of COD_{Mn}, DOC, and major nutrients in the four tributary bays of TGR. The results revealed a large spatial difference in COD_{Mn} across the tributary bays, as reflected by PXB (5.03 ± 6.24 mg·L^{-1}) > DNB (2.68 ± 1.57 mg·L^{-1}) > XXB (2.45 ± 1.26 mg·L^{-1}) > SNB (1.97 ± 1.54 mg·L^{-1}), showing a trend that the COD_{Mn} concentration increased in the tributary bay with increasing distance from the dam. The COD_{Mn} of PXB increased from the estuary to the upper reaches, with the maximum COD_{Mn} concentration reaching as high as 11.27 mg·L^{-1} (PX05), indicating that the upper reaches of PXB experienced severe organic pollution during the observation period. DOC characterizes the concentration of dissolved organic matter in terms of carbon content. During the observation period, the spatial trends of the DOC content and COD_{Mn} were generally similar, with PXB (2.29 ± 1.49 mg·L^{-1}) > DNB (1.74 ± 1.97 mg·L^{-1}) > SNB (1.62 ± 0.21 mg·L^{-1}) > XXB (1.45 ± 0.32 mg·L^{-1}), and the DOC waters increased with increasing distance from the dam. The spring nutrient concentrations in the four tributary bays showed that TN concentration varied little across the tributary bays and remained in the range of 0.88-2.40 mg·L^{-1}, with an average of 1.75 mg·L^{-1}, which was much higher than the commonly accepted eutrophication threshold (0.20 mg·L^{-1}) (Brown et al., 1998). The nitrogen species in the four tributary bays were dominated by NO_3^--N, with contents ranging from 0.24 to 1.40 mg·L^{-1}, and an average of 1.14 mg·L^{-1}. The NH_4^+-N concentrations in the four tributary bays ranged from 0.08 to 1.41 mg·L^{-1}, with an average of 0.17 mg·L^{-1}. There was an obvious difference in NH_4^+-N in the different tributaries, generally showing a descending order of PXB > DNB > SNB > XXB, and there was a high spatial difference in PXB, with a high NH_4^+-N concentration in the upper reaches. TP content was in the range of 0.01 to 0.31 mg·L^{-1}, with an average of 0.07 mg·L^{-1}, which was much higher than the commonly accepted eutrophication threshold (0.02 mg·L^{-1}) (Brown et al., 1998); overall, the TP content was relatively high in PXB and XXB.

Figure 7A shows the spatial distribution characteristics of TOC and TN in the sediments of the four tributary bays. The TOC ranged from 12.42 to 17.27 g·kg^{-1}, with an average of 14.11 g·kg^{-1}. Spatially, the closer a tributary bay is to the dam, the higher TOC in the sediments in the tributary bay. The TN content in the sediments was in the range of 0.29 to 0.48 g·kg^{-1}, with an average of 0.39 g·kg^{-1}. Except for the lower value (0.29 g·kg^{-1}) in DNB, the sediment TN contents of the other three bays differed little. There was a large difference in the C-to-N ratio in sediments in the tributary bays, showing an ascending order of PXB (31.67)< SNB (33.00)< XXB

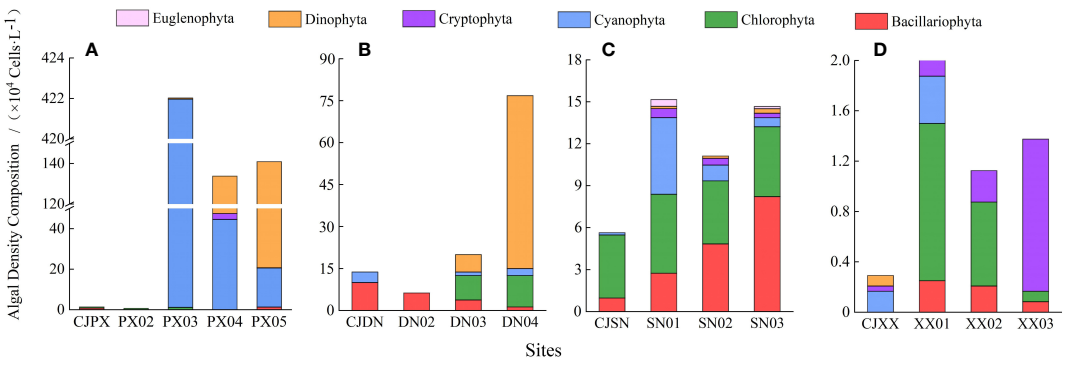

FIGURE 5
Composition of phytoplankton at different monitoring sites in each tributary bay [**(A)**, PXB; **(B)**, DNB; **(C)**, SNB; **(D)**, XXB].

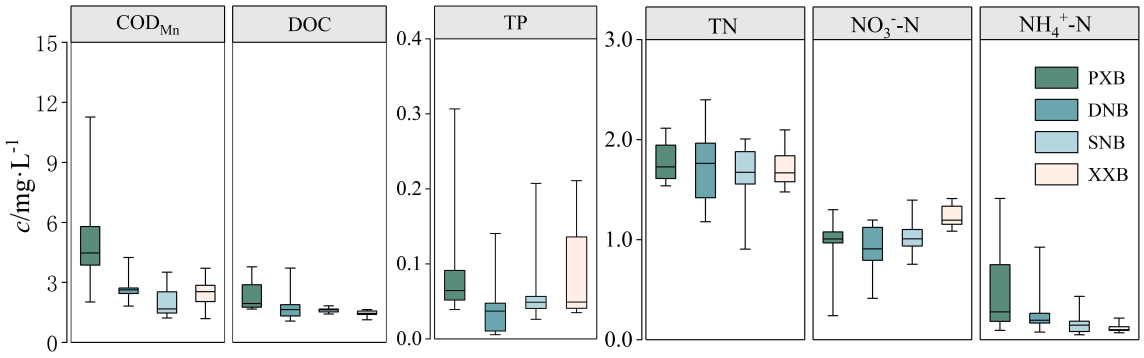

FIGURE 6
Spatial distribution of COD_{Mn}, DOC, and nutrient indicators in the different tributary bays.

(36.18)< DNB (47.04). A 48-hour laboratory oxygen demand simulation of sediments revealed a large spatial difference in SOC rate of the tributary bays in the TGR (Figure 7B), with a minimum of only 0.71 mg·m^{-2}·h^{-1} and a maximum of 22.05 mg·m^{-2}·h^{-1}. The average SOD rates in the different tributary bays were as follows: PXB (15.08 mg·m^{-2}·h^{-1}) > XXB (3.86 mg·m^{-2}·h^{-1}) > SNB (3.55 mg·m^{-2}·h^{-1}) > DNB (2.45 mg·m^{-2}·h^{-1}). The SOC rate in PXB and DNB increased initially and then decreased from the estuary to the upper reaches, with the largest rate occurring at PX03 and DN03 for each river, respectively; the SOC rate in SNB decreased from the estuary to the upper reaches, reaching its smallest rate at SN03 (1.06 mg·m^{-2}·h^{-1}), and the spatial characteristics of the SOC rate in XXB were unclear due to a relatively small number of monitoring sites.

3.5 CH_4 and CO_2 concentrations

To further investigate the spatial distribution characteristics of the GHG emissions in the different tributary bays, this study compared the differences in the CH_4 and CO_2 concentrations in the surface and bottom layers of the four tributary bays, as shown in Figure 8. The monitoring results showed that the CH_4 concentrations in the surface and bottom layers of PXB were generally higher than those in other tributary bays, with a higher concentration of CH_4 in the middle reaches (PX03-PX04); that the concentrations of CH_4 in DNB and SNB were both characterized by being low in the lower reaches and high in the upper reaches; and that the spatial characteristics of the CH_4 concentration in XXB were not clear due to the limited number of monitoring sites. Comparing the differences in CH_4 concentrations between the surface and bottom layers, it was found that the CH_4 concentrations in the bottom layers at PX03, PX04, DN03, DN04, SN02 and SN03 were higher than in the surface layers. These monitoring sites were the "sources" of CH_4 emissions. The CO_2 concentration also showed a decreasing trend in space, with the highest concentration in the upper reaches of PXB and the lowest concentration in the lower reaches of XXB. In addition, except for PXB, other tributaries had relatively high concentrations in the estuaries and relatively low concentrations inside the bays. In PXB and DNB, there was a significant difference between the CO_2 concentrations of the surface and bottom layers. The CO_2 concentration in the surface waters was generally lower than of the bottom layer, possibly due to the photosynthesis of planktonic algae.

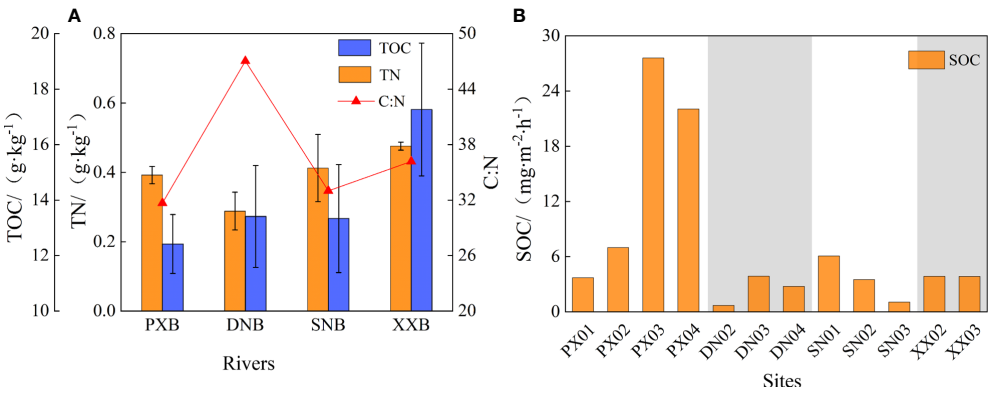

FIGURE 7
Sediment carbon and nitrogen distribution **(A)** and sediment oxygen demand rate **(B)** of the different tributary bays.

10.3389/fevo.2023.1297047

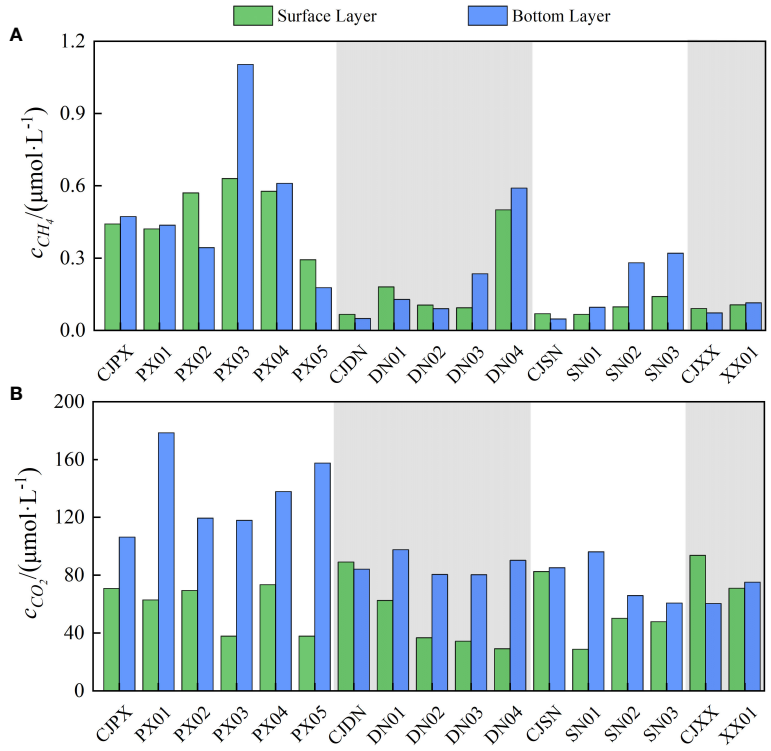

FIGURE 8
Spatial distribution characteristics of the CH_4 and CO_2 concentrations in the surface and bottom layers of the different tributary bays.

3.6 Cluster analysis of the mean values of physicochemical indicators

In this study, we found significant differences in the spatial characteristics of DO in the different tributary bays of the TGR during the same period. In PXB and DNB, DO showed a characteristic of more increasing stratification with the more distance from the dam, and in their bays, there was no obvious stratification in the estuary, strong stratification in the middle reaches, and weak stratification in the upper reaches (Figures 2A, B). In contrast, there was no clear vertical stratification of DO in the lower reaches of the SNB and XXB, and the spatial differences in the whole bay were not significant (Figures 2C, D). Furthermore, through the cluster analysis of the water environmental indicators of the four tributary bays in the same period (Figure 9), we found that the spring water environmental characteristics in four tributaries could be divided into four categories, and different categories corresponded to different DO stratification characteristics. The first category included the monitoring sites in SNB and XXB sections near the dam, where the water temperature was low, the water temperature stratification was weak, the water transparency was high, and the DO concentration was high and generally not stratified. The second category included monitoring sites DN02 to DN04 in the DNB, with DO stratification inside the tributary bay and DO supersaturation in the near-surface layer. Category 3 included DN01 and PX01 near the estuary of the tributary bay, and these sites were significantly affected by the mainstream waters of the Yangtze River and differed in terms of the thermal stratification and DO stratification state of the tributary bay. The fourth category included monitoring sites PX02 to PX05 in PXB, and its water environmental characteristics differed significantly from those of the other three categories, with obvious algal blooms, severe water pollution, and a large area of reservoir hypoxia.

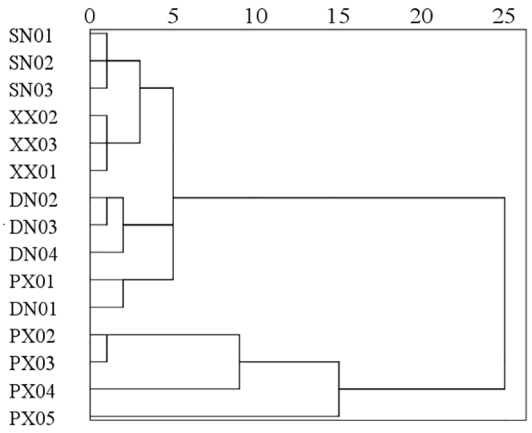

FIGURE 9
Cluster analysis of the mean values of water temperature, DO, nutrient indicators, COD_{Mn}, and DOC at each monitoring site in spring.

4 Discussion

4.1 Driving factors of spatial variabilities in DO

DO is a sensitive indicator reflecting changes in physical, chemical and biological processes in reservoir aquatic ecosystems (Foley et al., 2012; Zhang et al., 2015). Researchers (Correll, 1999; Zhang et al., 2015; Yan et al., 2017) have extensively examined oxygen consumption processes in reservoirs, considering physical, chemical, and biological perspectives while analyzing the evolutionary patterns of DO in these environments. Numerous studies have shown (Bocaniov et al., 2020; Zhang et al., 2020) that hypoxia in thermally stratified reservoirs is the result of a combination of factors such as hydrodynamics, thermal stratification, and external pollution loads.

Studies have found (Stefan et al., 1996; Jane and Rose, 2021) that thermal stratification played a dominant role in the evolution of DO stratification in lakes and reservoirs, which controls the vertical supply and migration of DO in waters. In this study we found that the spatial distribution of DO was consistent with the thermal stratification pattern of the bays (Figures 2, 3) and that the difference in thermodynamic processes was an important reason for the spatial difference in DO in the different tributary bays. The first category of waters, exemplified by SNB and XXB, was near the Three Gorges Dam and more significantly regulated by the reservoir discharge operation (Huang et al., 2017), which resulted in weak thermal stratification and intense vertical mixing in spring compared to the tributary bays in the upper reaches (Liu et al., 2016). This also resulted in the DO levels throughout the bays being similar to those in mainstream, without significant spatial differences. But there was DO stratification in the waters of the second category (DNB) and the fourth category (PXB), and the MOM phenomenon occurred at PX03 in PXB. In comparison, there was obvious thermal stratification in these two tributaries in spring (the average RWCS was 141.2 for PXB and 129.6 for DNB). Thus, the thermal stratification provided stable hydrodynamic conditions for the vertical stratification of DO. This is consistent with the findings from the 2020 study conducted in Hongjiadu Reservoir in Guizhou (Yu et al., 2020). It is notable that influenced by the backflowing water with high DO of the mainstream of the Yangtze River, the bottom water in the middle and upper reaches of PXB was replenished to some extent, the existence of the surface intrusion flow was an important reason for the formation of the MOM phenomenon. In addition, the low-temperature inflows from the upper reaches of DNB, SNB, and XXB all infiltrate the bottom part of the river channel as a downslope density flow (Figures 3B–D), with SpCond significantly negatively correlated with the DO of bottom waters (with R values of -0.806, -0.952, and -0.892, respectively, $P< 0.01$). This scenario played a role in replenishing the DO in the bottom layer of bays, while there were no significant low-temperature waters in the bottom layer of PXB.

Second, in addition to the influence of thermal stratification, water quality differences is an important reason of the spatial difference in DO stratification. COD_{Mn} and NH_4^+-N are the important indicator reflecting the degree of water pollution (Liu et al., 2020; Wang et al., 2022). In recent years, urbanization and industrial pollution in Kaizhou District, which is in the upper reaches of PXB, have increased the pollution load of the inflowing water to PXB (Chen et al., 2021). The relatively high COD_{Mn} concentration in the upstream inflow has exacerbated the oxygen consumption process in the reservoir bay. The higher concentration of NH_4^+-N in PXB than in the other tributaries indicated that its waters had been polluted recently (Liu et al., 2020), while the higher concentration of NH_4^+-N for nitrification reaction and oxygen consumption also reduced the DO concentration in the waters. Generally, COD_{Mn} and NH_4^+-N are negatively correlated with DO concentration. However, as shown in Supplementary Table S3, COD_{Mn} and NH_4^+-N were positively correlated with DO in the surface waters of PXB ($R = 0.833$, $P< 0.05$; $R = 0.917$, $P< 0.05$), while these correlations were not significant in the other tributaries. This correlation was not reasonable, mainly because the pollutant concentration gradually decreased when the inflow flowed from the surface layer to the lower reaches, and the DO concentration and thermal stratification of the surface waters and planktonic algae showed a decreasing trend from the upper to lower reaches, which also indicated that the DO of surface waters was mainly affected by thermal stratification and water quality.

It is reasonable that the COD_{Mn} was negatively correlated with DO in the bottom waters of PXB ($R=-0.830$, $P<0.01$), and the high concentration of organic pollutants (surface COD_{Mn} up to 11.27 $mg{\cdot}L^{-1}$) carried by the inflow from the upper reaches of PXB gradually sank while flowing toward the lower reaches (leading to an increase in the conductivity of the bottom waters, Supplementary Figure S2), which increased the pollution load of the bottom waters (with COD_{Mn} up to 5.89 $mg{\cdot}L^{-1}$ in the bottom layer), causing the oxygen consumption of middle and bottom waters to increase. In the upper reaches of the other tributaries, the pollution degree of the upstream incoming stream was low ($COD_{Mn}< 3$ $mg{\cdot}L^{-1}$) because industrial pollution was low, and waters with low conductivity and high DO replenished the middle and bottom waters through the downslope density flow in the bottom layer, which maintained the DO of the middle and bottom waters in the other tributaries at approximately 8 $mg{\cdot}L^{-1}$. Therefore, high pollution in the upper reaches significantly contributes to PXB's bottom water progressive hypoxia.

Finally, the differences in phytoplankton are also a significant factor contributing to the spatial differences in DO stratification (Zhang et al., 2015). Jane et al. analyzed (Jane et al., 2021) 393 temperate lakes and reservoirs from 1941 to 2017. They found that in relatively warmer and eutrophic lakes, surface dissolved oxygen was supersaturated. However, the deep-water oxygen concentrations in these reservoirs consistently remained low, likely due to the substantial sinking and decomposition of algae in the deeper zones of the water. In this study, a considerable volume of algae in the upper reaches of PXB gathered in the near-surface layer for photosynthesis, resulting in the supersaturation of DO in the surface and near-surface waters (with a maximum DO content of 17.47 $mg{\cdot}L^{-1}$ at PX04), followed by the algal biomass in DNB (with a maximum DO content of 13.30 $mg{\cdot}L^{-1}$ at PX04), while the DO content in the surface layers of SNB and XXB decreased to 10 $mg{\cdot}L^{-1}$ and 8 $mg{\cdot}L^{-1}$, respectively. Therefore, the difference in planktonic algal biomass was the main

reason for the difference in surface DO between different tributary bays.

In both PXB and DNB, the DO and DOC in the bottom waters were significantly negatively correlated (R=-0.920, P<0.01; R=-0.827, P<0.01). The DOC in water usually originates from phytoplankton or algae, and the decomposition of high-concentration DOC can consume a significant amount of DO (Wen et al., 2022). The oxygen-consuming decomposition of high-density algae after the decline in PXB was another key reason for accelerated hypoxia in the bottom waters. In 1979, Mitchell et al. (Mitchell and Burns, 1979) used a model to estimate the oxygen consumption of two eutrophic lakes in New Zealand, finding that organic matter decomposition plays the important role in oxygen consumption. Li et al.'s research (Li et al., 2023) in the Pearl River Estuary also confirmed that the highest underground chlorophyll values and the organic matter derived from them contribute to hypoxia. In contrast, although algal blooms occurred in DNB, dinoflagellates were the dominant species. Once cyanobacterial cells decline, they become more susceptible to oxygen-consuming microbial decomposition (Liu, 2019). After the decay of dinoflagellates, the decomposition rate of particulate total carbon (PTC) is relatively low. Therefore, the DO concentration in the bottom water remains relatively high. Furthermore, SOC plays a crucial role in reducing DO levels in water (Song et al., 2016). In this study, the SOC rate experiment revealed that the sediment TOC in the four tributary bays, except for XXB, did not show significant differences, but PXB exhibiting the highest sediment SOC content (Figure 7B). The comparison indicated that PXB had the lowest C:N value (Figure 7A), suggesting a relatively high proportion of endogenous organic carbon, particularly algal carbon in PXB's sediments (Wang, 2020). This further indicated that the difference in endogenous organic matter due to algal blooms emerged as a pivotal factor influencing the SOC rate (Yan et al., 2019). During the observation period, it's evident that the prevalence of cyanobacterial blooms in the upper reaches of the PXB significantly impacts the DO and SOC in the water, it is a factor that cannot be overlooked.

4.2 The vicious cycle among hypoxia, algal blooms and CH_4/CO_2 emissions

Since the impoundment of the TGR, algal blooms have occurred frequently in tributary bays (Stone, 2008; Yang et al., 2022). Accordingly, the dominant species of algal blooms in key tributaries evolved from channel-type algae dominated by Bacillariophyta and dinoflagellates in the early stage of impoundment to lake-type algae dominated by cyanobacteria and Chlorophyta (Liu et al., 2016; Yang et al., 2017; Yao et al., 2022). On the other hand, by comparing the results from different studies on the monitoring of DO in some tributary bays, we found that there was a clear decreasing trend of DO concentration in the water of the tributary bays of TGR in recent years. In addition, some bays have even shown significant hypoxic and anaerobic phenomena. At the beginning of the impoundment of the TGR (2009), the DO concentration was generally higher than 6 mg·L^{-1} in key tributary bays (Zhang et al., 2009), and there was no hypoxic or anaerobic phenomenon in the waters. By 2017, the waters of PXB had experienced long-term hypoxia (DO<4 mg·L^{-1}), and the DO concentration in the Modao Bay was as low as 5 mg·L^{-1} in spring and summer (Niu, X., 2019). In 2018, the DO concentrations at the bottom of XXB and SNB were as low as 4-5 mg·L^{-1} (Tian et al., 2022). In 2020, severe hypoxic and anaerobic phenomena (< 1 mg·L^{-1}) occurred in PXB (Ji et al., 2022). Therefore, under the background of continuous cyanobacterial blooms, hypoxic and anaerobic phenomena in waters have become another emerging water ecological environmental problem in the tributary bays of the TGR.

In this study, the closer a tributary bay was to the upper reaches, the more pronounced the degree of hypoxia, algal blooms and the higher the concentrations of CH_4 and CO_2 in the waters. Planktonic algae are an important factor affecting the carbon cycle of a reservoir ecosystem. In this type of ecosystem. When the algae decline and sink, they release fresh algal organic matter (AOM, Figure 10, ①) into the waters, and the oxygen-consuming decomposition of organic matter accelerates the consumption of DO in the subsurface and bottom waters (Figure 10, ②). A previous study (Zhang, 2015) showed that the decline in algal blooms not only promoted the formation of an anaerobic environment but also provided abundant reaction substrates for methanogenic microorganisms. Additionally, the density difference caused by water temperature stratification hinders the vertical transport and supply of DO, accelerating the hypoxic and anaerobic processes in the bottom waters, This intensifies the production of CH_4 under hypoxic and anaerobic conditions (Figure 10, ③). Therefore, the role of dead algae in promoting the production of CH_4 and CO_2 in rivers is significant. In addition, bottom CH_4 gradually oxidizes to CO_2 as it diffuses toward the water surface, a process that exacerbates hypoxia in the waters (Cai et al., 2010) (Figure 10, ④) and increases the concentration of CO_2 in the surface waters. This increase in CO_2 levels promotes algal growth (Figure 10, ⑤). Therefore, beginning with the outbreak and decline of algal blooms, the consumption of oxygen by water gradually intensifies. As hypoxic and anaerobic conditions in the waters worsen, emissions of CH_4 and CO_2 from reservoirs increase, further exacerbating the greenhouse gas effect of the reservoirs. And this, in turn, promotes the outbreak of algal blooms (Figure 10, ⑥), creating a reinforcing cycle (Yan et al., 2017).

Selecting PXB as an example, the CH_4 concentration in waters where cyanobacteria are generally high (PX03,1.10 μmol·L^{-1}), and in hypoxic waters with similar water environmental characteristics and similar phytoplankton biomass, the CH_4 concentration is higher in areas where cyanobacteria are the dominant species (PX04, PX05). which was much higher than those at other monitoring sites in this study and those in the results of a previous study of TGR (Liu et al., 2021). Therefore, the AOM contained in different dominant algae often varies, leading to diverse carbon behavior processes. A recent study (Liu, 2019) found that although the decline in *Cyclotella* sp. (Bacillariophyta), *Chlorella pyrenoidosa* (Chlorophyta), and *Microcystis aeruginosa* (Cyanobacteria) can all significantly contribute to the production of CH_4 and CO_2, different dominant algae have distinct fates for AOM. This is evident in the higher CO_2 release per unit of carbon

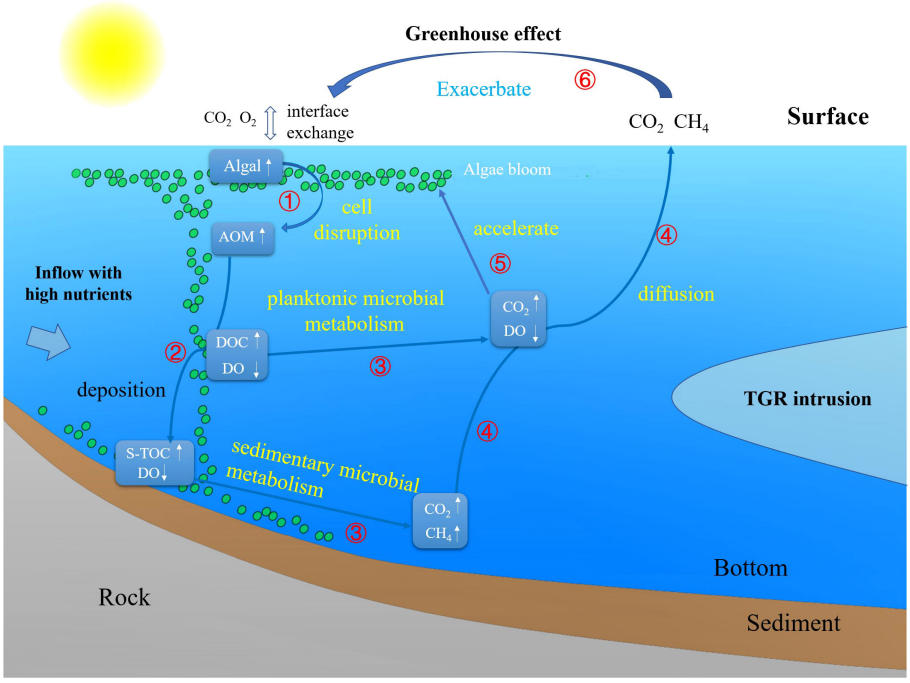

FIGURE 10
Schematic diagram of the processes of algal bloom formation and demise as well as GHG production and emissions in hypoxic reservoirs.

from *Cyclotella* sp. and the higher CH_4 release per unit of carbon from *Chlorella pyrenoidosa* and *M. aeruginosa*. It is well-known that the single-molecule global warming potential of CH_4 is 28 to 34 times that of CO_2 at a centennial scale (Williams et al., 2015). This suggests that, compared to other algal blooms, cyanobacterial and green algal blooms significantly contribute to the production of CH_4 in waters. If the frequency of outbreaks of cyanobacterial and green algal blooms increases, then the contribution of reservoirs to the greenhouse effect will also increase.

As mentioned above, the intense cycle among reservoir blooms, hypoxia, and GHG emissions should be a key reason for the spatial difference in the degree of algal blooms, water hypoxia, and GHG emissions in different tributary bays in this study. Similarly, related studies have further confirmed this finding. Sun (Sun et al., 2020) statistically analyzed the GHG emission fluxes of the mainstream and tributaries of the TGR from 2010 to 2017 and found that in the tributary backwater areas with higher eutrophication, larger CH_4 fluxes occurred with increased frequency, and the CH_4 yield was greater during water bloom outbreaks. In Zhushan Bay of Taihu lake, the surface water in the bloom areas of cyanobacterial blooms has a CH_4 concentrations as high as 3.79 $\mu mol \cdot L^{-1}$, significantly higher than in other areas (Yan et al., 2019). Other study (Liu, 2019) has found that compared to Bacillariophyta (*Cyclotella* sp.), the outbreak of lake-type cyanobacterial (*M. aeruginosa*) significantly promotes the production of CH_4 in sediments, thereby favoring the release of CH_4 into the water. Yan et al. (Yan et al., 2017) simulated the decomposition process of cyanobacterial blooms and further confirmed the presence of a strong cycle between cyanobacterial blooms, eutrophication, and GHGs in lakes. Therefore, the phenomenon of water bloom in reservoir and the evolvement process of their dominant species have a nonnegligible impact on carbon cycle. The metabolic substrates and the anaerobic environment created by the dead algae will significantly contribute to the production of CH_4 and CO_2 in rivers. As a result, algal bloom and succession caused by building dam in river have a strong positive feedback effect on water hypoxia, anaerobic processes, and greenhouse effects. Based on this understanding, the prevention and control of cyanobacterial blooms in reservoirs can, to some extent, improve the difference in and cycle of carbon in reservoirs. Consequently, this holds significant impact in mitigating the global greenhouse effect.

5 Conclusions

There were notable spatial differences in the water environmental characteristics of the four different tributary bays of the TGR, especially in terms of hypoxia and algal blooms. The spatial differences of DO were closely related to hydrodynamics, planktonic algae, and inflow pollution loads. The thermal stratification in PXB provided stable hydrodynamic conditions, resulting in hypoxia in the subsurface-bottom reach of the bay, and the intrusion flow from the mainstream significantly replenished DO in the middle layer of the bay. The downslope density current in the upper reaches of DNB, SNB, and XXB, to some extent, replenished DO in the bottom layer. The high pollution load was also an important driver of progressive hypoxia in PXB. In addition, the contribution of cyanobacteria, as the dominant species of algal blooms in PXB, to aerobic degradation and reservoir hypoxia cannot be ignored. The study also found that

the water CH_4 concentration was higher where cyanobacteria dominated in PXB. The succession process of algal blooms and their dominant species had a nonnegligible influence on the river carbon cycle process. The metabolic substrates released by and the anaerobic environment created by the decline in algae will significantly promote the production of CH_4 and CO_2 in rivers. The algal blooms and algal succession caused by river damming have a strong positive feedback effect on reservoir hypoxia, anaerobic processes, and greenhouse effects.

Data availability statement

The original contributions presented in the study are included in the article/Supplementary Material. Further inquiries can be directed to the corresponding author.

Ethics statement

The manuscript presents research on aquatic ecological environments that do not require ethical approval for their study.

Author contributions

DJ: Conceptualization, Data curation, Funding acquisition, Writing – original draft, Formal analysis, Investigation, Methodology, Project administration, Resources, Software, Visualization. YHa: Investigation, Methodology, Software, Writing – original draft, Conceptualization, Data curation, Formal analysis, Visualization. LL: Methodology, Supervision, Writing – original draft, Writing – review & editing. XX: Formal Analysis, Project administration, Writing – review & editing. HX: Formal analysis, Investigation, Methodology, Writing – review & editing. SQ: Data curation, Investigation, Resources, Software, Writing – review & editing. JM: Formal analysis, Methodology, Validation, Visualization, Writing – review & editing. XZ: Formal Analysis, Resources, Writing – review & editing. YHu: Project administration, Validation, Visualization, Writing – review & editing. DL: Conceptualization, Writing – review & editing.

Funding

The author(s) declare financial support was received for the research, authorship, and/or publication of this article. This work is financially supported by the Natural Science Foundation of China (grant Nos. U2040220, 52079069, 52009066, 52379069). The Natural Science Foundation of Hubei Province (2022CFB807) and open fund of Engineering Research Center of Eco-Environment in Three Gorges Reservoir Region, Ministry of Education (KF2022-06) and Major Program of Science and Technique of Chinese Ministry of Water Resources (SKS-2022077) both provided additional financial support for the field measurements.

Conflict of interest

The authors declare that the research was conducted in the absence of any commercial or financial relationships that could be construed as a potential conflict of interest.

Publisher's note

Supplementary material

The Supplementary Material for this article can be found online at: https://www.frontiersin.org/articles/10.3389/fevo.2023.1297047/full#supplementary-material

References

Bocaniov, S. A., Lamb, K. G., Liu, W., Rao, Y. R., and Smith, R. E. H. (2020). High sensitivity of lake hypoxia to air temperatures, winds, and nutrient loading: insights from a 3-D lake model. *Water Resour. Res.* 56 (12), 1–27. doi: 10.1029/2019WR027040

Brown, C. D., Canfield, D. E., Bachmann, R. W., and Hoyer, M. V. (1998). Seasonal patterns of chlorophyll, nutrient concentrations and secchi disk transparency in Florida lakes. *Lake Reservoir Manage.* 14, 60–76. doi: 10.1080/07438149809354110

Cai, W. J., Luther, G. W., Cornwell, J. C., and Giblin, A. E. (2010). Carbon cycling and the coupling between proton and electron transfer reactions in aquatic sediments in Lake Champlain. *Aquat. Geochem.* 16 (3), 421–446. doi: 10.1007/s10498-010-9097-9

Cao, Y., Wen, S., and Wang, X. (2022). Sediment oxygen demand and the overlying water oxygen deficit in Lake Baiyangdian. *Acta Scientiae Circumstantiae* 42, 02, 240–248. doi: 10.13671/j.hjkxxb.2021.0135

Chen, X., Zhang, W., Yin, Y., Tang, J., Li, G., and Yan, Y. (2021). Seasonal variation characteristics and release potential of phosphorus in sediments: a case study of the Qiuxi River, a typical diffuse source pollution river in Southwestern China. *J. Soils Sediments* 21 (1), 575–591. doi: 10.1007/s11368-020-02805-x

Correll, D. L. (1999). Phosphorus: a rate limiting nutrient in surface waters. *Poultry Sci.* 78 (5), 674–682. doi: 10.1093/ps/78.5.674

Ding, Y., Wang, H., Zhang, Q., Chai, B., Lei, X., Ye, M., et al. (2022). Effects of dissolved oxygen on phosphorus transformation in reservoir sediments: novel insights on bacterial community and functional genes. *J. Soils* 22, 2094–2104. doi: 10.1007/s11368-022-03233-9

Foley, B., Jones, I. D., Maberly, S. C., and Rippey, B. (2012). Long-term changes in oxygen depletion in a small temperate lake: effects of climate change and eutrophication. *Freshw. Biol.* 57 (2), 278–289. doi: 10.1111/j.1365-2427.2011.02662.x

Huang, W. M., Bi, Y. H., Hu, Z. Y., Zhu, K. X., Zhao, W., and Yuan, X. G. (2015). Spatio-temporal variations of GHG emissions from surface water of Xiangxi River in Three Gorges Reservoir region, China. *Ecol. Eng.* 83, 28–32. doi: 10.1016/j.ecoleng.2015.04.088

Huang, Y., Ji, D., and Long, L. (2017). The variance analysis of characteristics and blooms of the typical tributaries of the three gorges reservoir in spring. *Resources and Environment in the Yangtze Basin* 26, 03, 461–470. doi: 10.11870/cjlyzyyhj201703017

Jaiswal, D., Naaz, N., Gupta, S., Madhav, K., and Pandey, J. (2023). Diurnal oscillation in dissolved oxygen at sediment-water interface fuels denitrification-driven N removal in Ganga River. *J. Hydrol.* 619, 129301. doi: 10.1016/j.jhydrol.2023.129301

Jane, S. F., Hansen, G. J. A., Kraemer, B. M., Leavitt, P. R., Mincer, J. L., North, R. L., et al. (2021). Widespread deoxygenation of temperate lakes. *Nature* 594 (7861), 66–70. doi: 10.1038/s41586-021-03550-y

Jane, S. F., and Rose, K. C. (2021). Predicting arctic-alpine lake dissolved oxygen responses to future tree line advance at the Swedish forest-tundra transition zone. *Global Change Biol.* 27 (18), 4207–4209. doi: 10.1111/gcb.15748

Ji, D., Fang, J., and Long, L. (2022). Characteristics and dfferences of dissolved oxygen stratification in different tributaries of three gorges reservoir during impoundment period. *Environ. Sci.* 43 (07), 3543–3551. doi: 10.13227/j.hjkx.202109244

Kai, W. (2020). Dynamic process and control factors of dissolved organic matter in Xiangxi Bay of Three Gorges Reservoir Zhejiang University.

Li, D., Gan, J., Lu, Z., Cheng, W., Kung, H., and Li, J. (2023). Hypoxia formation triggered by the organic matter from subsurface chlorophyll maximum in a large estuary-shelf system. *Water Res.* 240, 120063. doi: 10.1016/j.watres.2023.120063

Li, Z., Ma, J., Guo, J., Paerl, H. W., Brookes, J. D., Xiao, Y., et al. (2019). Water quality trends in the Three Gorges Reservoir region before and after impoundment, (1992–2016). *Ecohydrol. Hydrobiol.* 19 (3), 317–327. doi: 10.1016/j.ecohyd.2018.08.005

Liu, C., Liu, X., and Zhou, H. (2019). Temporal and spatial evolution characteristics and driving factors of reservoir anoxic zone. *J. Hydraulic Eng.* 50 (12), 1479–1490.

Liu, D., Yang, Z., and Ji, D. (2016). A review on the mechanism and its controlling methods of the algal blooms in the tributaries of Three Gorges Reservoir. *J. Hydraulic Eng.* 47 (03), 443–454. doi: 10.13243/j.cnki.slxb.20151304

Liu, J., Xiao, S., Wang, C., Yang, Z., Liu, D., Guo, X., et al. (2021). Spatial and temporal variability of dissolved methane concentrations and diffusive emissions in the Three Gorges Reservoir. *Water Res.* 207, 117788. doi: 10.1016/j.watres.2021.117788

Liu, S., Yuan, X., and Wang, X. (2020). patiotemporal distribution and influencing factors of nitrogen and phosphorus in water column of Hanfeng Lake and Gaoyang Lake. *China Environ. Sci.* 40 (11), 4965–4973. doi: 10.19674/j.cnki.issn1000-6923.2021.0331

Liu, Y. (2019). *Transformation and fate of carbon caused by algae decay in the Yulin river* (Chongqing: Three Gorges Reservoir A rea Chongqing University).

Lv, K., Guo, X., Wang, C., Su, Q., Liu, D., Xiao, S., et al. (2022). Sediment nitrogen contents controlled by microbial community in a eutrophic tributary in Three Gorges Reservoir, China. *Environ. pollut.* 314, 120312. doi: 10.1016/j.envpol.2022.120312

Mi, C., Shatwell, T., Ma, J., Wentzky, V. C., Boehrer, B., Xu, Y., et al. (2020). The formation of a metalimnetic oxygen minimum exemplifies how ecosystem dynamics shape biogeochemical processes: A modelling study. *Water Res.* 175 (May15), 115701. doi: 10.1016/j.watres.2020.115701

Mitchell, S. F., and Burns, C. W. (1979). Oxygen consumption in the epilimnia and hypolimnia of two eutrophic, warm-monomictic lakes. *New Z. J. Mar. Freshw. Res.* 13 (3), 427–441. doi: 10.1080/00288330.1979.9515820

Picard, A., Gartman, A., Cosmidis, J., Obst, M., Vidoudez, C., Clarke, D. R., et al. (2019). Authigenic metastable iron sulfide minerals preserve microbial organic carbon in anoxic environments. *Chem. Geol.* 530, 119343. doi: 10.1016/j.chemgeo.2019.119343

Qu, L., He, C., Wu, Z., Dahlgren, R. A., Ren, M., Li, P., et al. (2022). Hypolimnetic deoxygenation enhanced production and export of recalcitrant dissolved organic matter in a large stratified reservoir. *Water Res.* 219, 118537. doi: 10.1016/j.watres.2022.118537

Rucinski, D. K., DePinto, J. V., Beletsky, D., and Scavia, D. (2016). Modeling hypoxia in the central basin of Lake Erie under potential phosphorus load reduction scenarios. *J. Great Lakes Res.* 42 (6), 1206–1211. doi: 10.1016/j.jglr.2016.07.001

Schindler, D. (2006). Recent advances in the understanding and management of eutrophication. *Limnol. Oceanogr.* 51, 356–363. doi: 10.4319/lo.2006.51.1_part_2.0356

Shen, Z.-y., Hong, Q., Yu, H., and Niu, J.-F. (2010). Parameter uncertainty analysis of non-point source pollution from different land use types. *Sci. Total Environ.* 408 (8), 1971–1978. doi: 10.1016/j.scitotenv.2009.12.007

Siegel, D. A., Doney, S. C., and Yoder, J. A. (2002). The North atlantic spring phytoplankton bloom and sverdrup's critical depth hypothesis. *Science* 296 (5568), 730–733. doi: 10.1126/science.321.5889.628

Song, G., Liu, S., Zhu, Z., Zhai, W., Zhu, C., and Zhang, J. (2016). Sediment oxygen consumption and benthic organic carbon mineralization on the continental shelves of the East China Sea and the Yellow Sea. *Deep Sea Res. Part II: Topical Stud. Oceanogr.* 124, 53–63. doi: 10.1016/j.dsr2.2015.04.012

Stefan, H. G., Hondzo, M., Fang, X., Eaton, J. G., and McCormick, J. H. (1996). Simulated long term temperature and dissolved oxygen characteristics of lakes in the north-central United States and associated fish habitat limits. *Limnol. Oceanogr.* 41 (5), 1124–1135. doi: 10.4319/lo.1996.41.5.1124

Stone, R. (2008). Three gorges dam: into the unknown. *Science* 321 (5889), 628–632.

Sun, Z., Chen, Y., and Li, C. (2020). Research of reservoir greenhouse gas; emissions in China, (2009-2019):Review and outlook. *J. Hydraulic Eng.* 51 (03), 253–267. doi: 10.13243/j.cnki.slxb.20190478

Sun, H., Lu, X., Yu, R., Yang, J., Liu, X., Cao, Z., et al. (2021). Eutrophication decreased CO2 but increased CH4 emissions from lake: A case study of a shallow Lake Ulansuhai. *Water Res.* 201, 117363. doi: 10.1016/j.watres.2021.117363

Tian, P., Li, Y., and Li, Y. (2022). Effects of three gorges reservoir operation on vertical distribution of chlorophyll a and environmental factors in tributaries. *Environ. Sci.* 43 (01), 295–305. doi: 10.13227/j.hjkx.202105201

Wang, C., Zhang, H., Lei, P., Xin, X., Zhang, A., and Yin, W. (2022). Evidence on the causes of the rising levels of CODMn along the middle route of the South-to-North Diversion Project in China: The role of algal dissolved organic matter. *J. Environ. Sci.* 113, 281–290. doi: 10.1016/j.jes.2021.06.003

Wen, G., Wang, S., and Cao, R. (2022). A review of the formation causes, ecological risks and water quality responses of metal-imnetic oxygen minimum in lakes and reservoirs. *J. Lake Sci.* 34 (03), 711–726. doi: 10.18307/2022.0301

Wetzel, R. G. (2001). Limnology: lake and river ecosystems. *Eos Trans. Am. Geophysical Union* 21 (2), 1–9. doi: 10.1016/B978-0-08-057439-4.50017-4

Williams, A. P., Seager, R., Abatzoglou, J. T., Cook, B. I., Smerdon, J. E., and Cook, E. R. (2015). Contribution of anthropogenic warming to California drought during 2012-2014. *Geophysical Res. Lett.* 42 (16), 6819–6828. doi: 10.1002/2015GL064924

Xiaoxu, N. (2019). *Comparison of environmental difference between Pengxi and Modao River in the Three Gorges Reservoir based on severity of algal blooms* (Southwest University).

Xue, J., Yao, X., Zhao, Z., He, C., Shi, Q., and Zhang, L. (2021). Internal loop sustains cyanobacterial blooms in eutrophic lakes: Evidence from organic nitrogen and ammonium regeneration. *Water Res.* 206, 117724. doi: 10.1016/j.watres.2021.117724

Yan, X., Xu, X., Ji, M., Zhang, Z., Wang, M., Wu, S., et al. (2019). Cyanobacteria blooms: A neglected facilitator of CH4 production in eutrophic lakes. *Sci. Total Environ.* 651, 466–474. doi: 10.1016/j.scitotenv.2018.09.197

Yan, X., Xu, X., Wang, M., Wang, G., Wu, S., Li, Z., et al. (2017). Climate warming and cyanobacteria blooms: Looks at their relationships from a new perspective. *Water Res.* 125, 449–457. doi: 10.1016/j.watres.2017.09.008

Yang, Z., Wei, C., Liu, D., Lin, Q., Huang, Y., Wang, C., et al. (2022). The influence of hydraulic characteristics on algal bloom in Three Gorges Reservoir, China: A combination of cultural experiments and field monitoring. *Water Res.* 211, 118030. doi: 10.1016/j.watres.2021.118030

Yang, Z., Y., Y., and Chen, Z. (2017). Mechanism of eutrophication and phytoplankton blooms in Three Gorges Reservoir, China: A research review. *Eng. J. Wuhan Univ.* 50 (04), 507–516. doi: 10.14188/j.1671-8844.2017-04-005

Yao, J., Fan, X., and Yang, X. (2022). Current situation, causes and control measures of water bloom in the key tributaries of the three gorges reservoir. *Chin. J. Environ. Eng.* 16 (06), 2041–2048. doi: 10.12030/j.cjee.202112199

Yu, J., Chen, J., Zeng, Y., Lu, Y., and Chen, Q. (2020). Carbon and phosphorus transformation during the deposition of particulate matter in the large deep reservoir. *J. Environ. Manage.* 265, 110514. doi: 10.1016/j.jenvman.2020.110514

Zhang, Y. (2015). Effect of climate warming on lake thermal and dissolved oxygen stratifications: A review. *Adv. Water Sci.* 26 (01), 130–139. doi: 10.14042/j.cnki.32.1309.2015.01.017

Zhang, Y., Arhonditsis, G., Chen, Q., and Peng, J. (2020). The magnitude and drivers of harmful algal blooms in China's lakes and reservoirs: A national-scale characterization. *Water Res.* 181, 115902. doi: 10.1016/j.watres.2020.115902

Zhang, S., Li, C., and Zheng, J. (2009). Seasonal V ariation of trophic states in backwater areas of tributaries in three gorges reservoir. *Environ. Sci.* 30 (01), 64–69. doi: 10.13227/j.hjkx.2009.01.037

Zhang, Y., Wu, Z., Liu, M., He, J., Shi, K., Zhou, Y., et al. (2015). Dissolved oxygen stratification and response to thermal structure and long-term climate change in a large and deep subtropical reservoir (Lake Qiandaohu, China). *Water Res.* 75 (may 15), 249–258. doi: 10.1016/j.watres.2015.02.052

Zhang, J., Zeng, Y., and Zhao, Y. (2011). Threshold analysis of water blooms in Baiyangdian wetlands. *Chin. J. Ecol.* 30 (08), 1744–1750. doi: 10.13292/j.1000-4890.2011.0257